Text and references accompanying Nevada Bureau of Mines and Geology Open-File Report 20-3

Geologic Map of the North Half of the Tent Mountain Quadrangle, Elko County, Nevada

by

Andrew V. Zuza[1], Seth Dee[1], and Benjamin J.C. Laabs[2]

[1]Nevada Bureau of Mines and Geology, University of Nevada, Reno
[2] Department of Geosciences, North Dakota State University

2020

Disclaimer: NBMG open-file reports are preliminary. They have not been thoroughly edited or peer reviewed. This geologic map was funded in part by the USGS National Cooperative Geologic Mapping Program under STATEMAP award number G19AC00383, 2019.

DESCRIPTION OF MAP UNITS

Quaternary Deposits

Qc Colluvium (Holocene) Unconsolidated, angular to slightly rounded boulders to pebbles of bedrock in a variably sandy matrix. Commonly 1–5 m thick.

Qls Landslide deposits (Holocene to Pleistocene) Minor slope failure deposits with a wide range of characteristics and compositions. Locally dominated by highly fractured or jumbled bedrock, with a varying percentage of poorly to moderately sorted gravels and fines. Typically form uneven, hummocky surfaces. Head scarps vary from sharp and fresh to rounded and indistinct.

Qlsm Slide block of marble in landslide deposit (Holocene to Pleistocene) Displaced landslide blocks of marble bedrock within a Qls deposit.

Qay Active alluvium (Holocene) Deposits of mud, silt, sand, and pebble- to cobble-sized gravel in active and ephemeral channels and floodplains.

Qfy_1 Youngest alluvial-fan deposits (late Holocene) Deposits of silt, sand and pebble- to cobble- sized gravel in active alluvial fans and active ephemeral stream channels. Includes subrounded to subangular clasts of mylonitic quartzite, gneiss, and granitic rocks derived from the East Humboldt Range. Surfaces are generally smooth at mid- and distal-fan locations but have subtle bar and swale morphology near fan heads and within active channels. Slightly inset below adjacent Qfy_2 deposits but with prominent topographic separation from older deposits. Post-dates most recent surface rupturing earthquake on the Ruby Mountains fault.

Qfy_2 Young alluvial-fan deposits (middle to early Holocene) Deposits of silt, sand and pebble- to cobble-sized gravel in generally inactive alluvial fans. Includes subrounded to subangular clasts of mylonitic quartzite, gneiss, and granitic rocks derived from the East Humboldt Range. Surfaces are generally planar and mildly dissected by gully incision. Well preserved near the mouths of drainages, where the unit has been uplifted 1–2.5 m in the footwall of the Ruby Mountains fault by the most recent surface rupturing earthquake. Carbon obtained from the unit in a paleoseismic trench at Reed Creek yielded an age of 7500 + 70 cal yr B.P (Wesnousky and Willoughby, 2003).

Qfy Young alluvial-fan deposits, undivided (Holocene) Deposits of silt, sand and pebble- to cobble- sized gravel in alluvial fans and ephemeral stream channels. Includes undivided Qfy_1 and Qfy_2.

Qfi Intermediate-age alluvial-fan deposits (late Pleistocene) Deposits of silt, sand, and pebble- to cobble-sized gravel with boulders. Includes subrounded to subangular clasts of mylonitic quartzite, gneiss, and granitic rocks derived from the East Humboldt Range. Surfaces are broadly rounded, dissected, and topographically separated from Qfy deposits. Well preserved on terraces beveled onto Ts deposits in the footwall of the Ruby Mountains fault. Absent at the mouths of glaciated drainages suggesting Qfi may be time correlative with glacial outwash deposits associated with latest Pleistocene Angel Lake glaciation (Qgo_1).

Qgo_1 Glacial outwash deposits (late Pleistocene) Deposits of silt, sand, and pebble-to cobble-sized gravel with boulders up to 3 m in diameter. Includes rounded to subrounded clasts of mylonitic quartzite, gneiss, and granitic rocks. Alluvial outwash from the Angel Lake glacial advance.

Cosmogenic ^{10}Be exposure ages of boulders atop a correlative Qgo_1 surface at the mouth of Greys Creek in the adjacent Herder Creek 7.5' quadrangle have two groupings of ages (table 1 and fig. 1). A grouping of three boulders with exposure ages ranging from 14–27 ka, which corresponds with previously published ages from glacial deposits of the last glaciation in the Ruby Mountains–East Humboldt Range (Laabs et al., 2020). This is the preferred age for the Qgo_1 geomorphic surface and suggests that the outwash surface is correlated to the Angel Lake glaciation (as termed by Sharp, 1938). Another grouping of three boulders with ages ranging from 65–81 ka suggest a period of aggradation that may be associated with glaciation that is not well preserved in the moraine record.

Qgm_1 Glacial moraine deposits (late Pleistocene) Deposits of poorly sorted sand, gravel, and boulders up to 6 m in diameter forming lateral moraines from the Angel Lake glacial advance, moraine crests shown. Includes subangular to subrounded clasts of mylonitic quartzite, gneiss and granitic rocks. Moraine crests are sharp with abundant boulders. Locally inset adjacent to Lamoille age moraines.

Qgo_2 Glacial outwash deposits (middle Pleistocene) Deposits of silt, sand, and pebble-cobble gravel with boulders up to 6 m in diameter. Includes rounded to subrounded clasts of mylonitic quartzite, gneiss and granitic rocks. Alluvial outwash is likely from the middle Pleistocene Lamoille glacial advance.

Cosmogenic 10Be exposure ages of boulders atop a Qgo_2 surface at the mouth of Boulder Creek in the Tent Mountain 7.5' quadrangle have two groupings of ages (table 1 and fig. 1). A grouping of three boulders with minimum ages ranging from 120–130 ka (zero-erosion ages) which corresponds with previously published dates from glacial deposits of the penultimate glaciation in the Ruby Mountains–East Humboldt Range (Laabs et al., 2020). This is the preferred age for the Qgo_2 geomorphic surface at Boulder Creek and suggests that the outwash surface is correlated to the Lamoille glaciation (as termed by Sharp, 1938). Another grouping of three boulders on the Boulder Creek surface have ages ranging from 23–31 ka which suggest that the Qgo_2 surface was not entirely abandoned during the Angel Lake glaciation. Seven additional boulders were sampled from a correlative Qgo_2 surface at the mouth of Greys Creek with a grouping of 5 boulders with ages ranging from 124–204 ka.

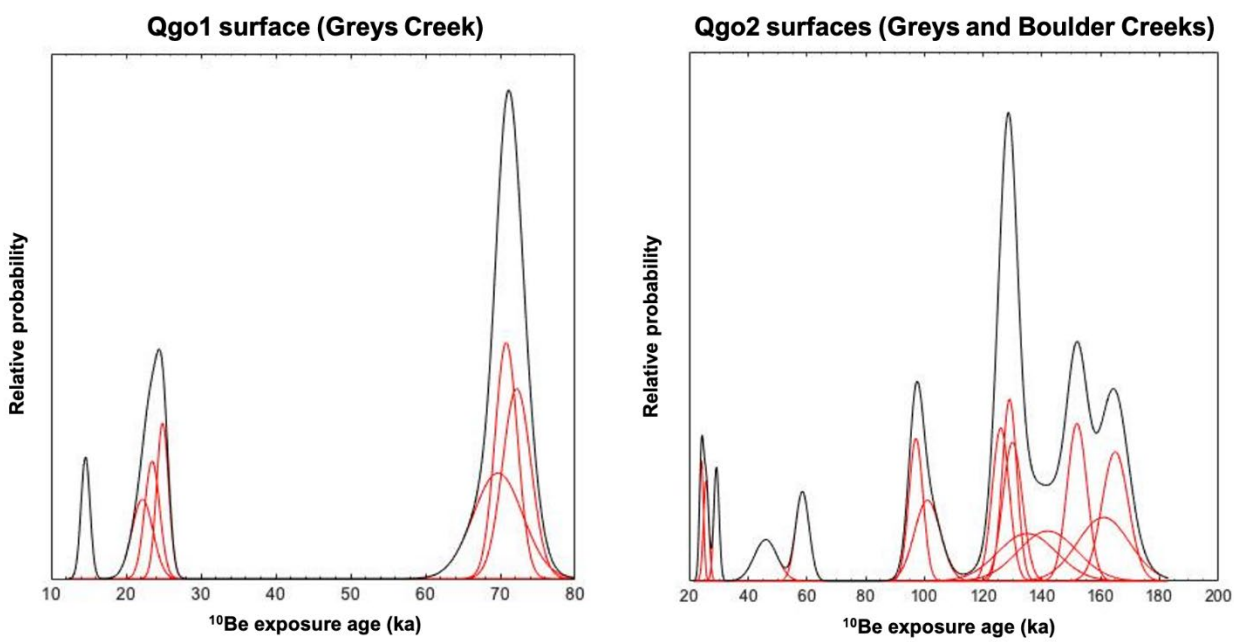

Figure 1. Cumulative probability distribution curves of surface-exposure ages of boulders deposited on Qgo_1 and Qgo_2 surfaces at the mouths of Greys and Boulder Creeks in the Tent Mountain and Herder Creek quadrangles. Data in table 1.

Qgm_2 Glacial moraine deposits (middle Pleistocene) Deposits of poorly sorted sand, gravel, and boulders up to 6 m in diameter forming lateral moraines likely from the middle Pleistocene Lamoille glacial advance, moraine crests shown. Includes subangular to subrounded clasts of mylonitic quartzite, gneiss and granitic rocks. Moraine crests are rounded with fewer boulders exposed on the crest than Qgm_1.

Qsp Sag pond (Holocene to Pleistocene) Fine-grained deposits preserved behind rotated slide blocks or in depressions on hummocky landslide deposits.

Qmlsrcp, Qmlsrfp Slide block of coarsely or finely porphyritic rhyolite in Quaternary mega-landslide deposit (middle Pleistocene?) Displaced landslide blocks of units Trcp and Trfp within a Pleistocene mega-landslide. See unit description for Trcp below.

Qmlss Slide block of tuffaceous sedimentary rock in Quaternary mega-landslide deposit (middle Pleistocene?) Displaced landslide blocks of unit Ts within a Pleistocene mega-landslide. See unit description for Ts below.

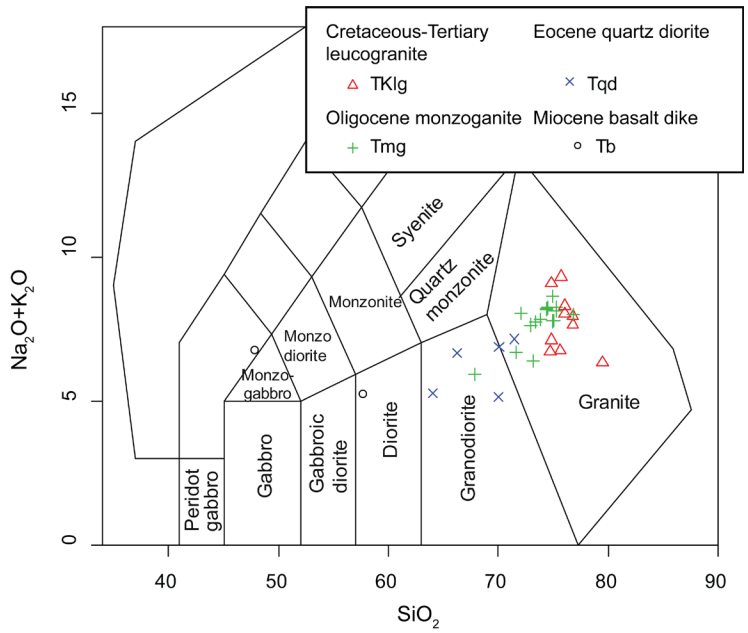

Figure 2. New geochemical data for samples analyzed in the Tent Mountain quadrangle, or just east in the Humboldt Peak quadrangle. Data in table 3. Data plotted in a total alkalis versus silica (TAS) diagram of Middlemost (1994). Some samples were collected and analyzed by D. A. Levy.

Qfo_1, Qfo_2, Qfo_3 Older alluvial-fan deposits (middle Pleistocene) Deposits of silt, sand, and pebble- to cobble sized gravels with boulders up to 2 m diameter. Includes subrounded to subangular clasts of mylonitic quartzite, gneiss, and granitic rocks, derived from the East Humboldt Range. Soil development varies, with stage III Bk and/or Bt horizons locally up to 0.3 m thick. Three distinct and topographically correlative terrace and pediment surfaces (Qfo_1, Qfo_2, and Qfo_3) are preserved on the uplifted footwall of the Ruby Mountains fault along the west side of the East Humboldt Range. South of Herder Creek, Qfo surfaces are beveled on to Tertiary sediments and to the north they are preserved as small remnants deposited on crystalline bedrock. Qfo_3 is a regionally extensive surface that Sharp (1940) named the "Lee" surface.

Qmls Mega-landslide deposit (middle Pleistocene?) Undivided mega-landslide deposit with intermixed, blocks of quartzite, leucogranite, monzogranite, and marble up to 10 m long. Forms uneven hummocky surface on the west flank of Tent Mountain. Fault scarps are present in the westernmost toe of the deposit. Adjacent, unfaulted deposits of Qfo_3 must be younger in age and inset against the landslide deposit.

Tertiary Sedimentary Rocks

Ts Tertiary sedimentary rocks, undivided (Pliocene to Miocene) A heterogeneous sequence of tuffaceous sandstone, siltstone, conglomerate, tephra, minor diatomite, and lacustrine sediments at least part of which is the middle Miocene Humboldt Formation but in the Herder Creek quadrangle likely includes younger deposits in the basin west of the Ruby Mountains fault. All of the deposits are non-resistant and very poorly exposed, thus hindering development of a comprehensive stratigraphy.

The most common rock types in Ts are well-bedded to platy, variably calcite-cemented, fine- to coarse-grained, commonly tuffaceous sandstone and siltstone. Fragments of quartz, feldspar, and chert are the main constituents. Outcrops are sparse, and these rocks are mostly encountered as 1–2 cm angular chips of tan or white float, including some diatomite. Fluvial, pebble-cobble conglomerates are sparsely interbedded with sandstone and siltstone throughout the section. Conglomerate clast types vary but locally include subrounded to well-rounded, non-foliated Paleozoic sedimentary rocks, gneiss, mylonitic quartzite, and mylonitic granitic rocks. Conglomerates commonly occur as nested channels, 2–10 m wide and 1–2 m thick with no outcrop exposed above or below.

Horizons of white and silvery gray tephra occur throughout the section. Discrete tephra horizons range in thickness from 15 cm to ~3 m, and composite sections of layered and variably reworked tephra are locally >5 m thick. Age constraints for Ts consist of $^{40}Ar/^{39}Ar$ ages summarized in table 2 from the Herder Creek, Heelfly Creek, and Tent Mountain quadrangles. Tephra dated in this map area (sample GD14-116B), from depositionally beneath 15.33 Ma rhyolite lava flows (Trcp), yielded an age of 15.77±0.02 Ma from 15 anorthoclase grains (out of 20 analyses). Other tephra ages from a variety of analyzed phases from adjacent quadrangles span 16 Ma to 8 Ma (table 2). In the Herder Creek quadrangle to the north (Dee and Ressel, 2016), two samples of Ts from a continuous stratigraphic section yielded maximum depositions of ca. 23 Ma for the lower sample and ca. 5 Ma for the upper sample (table 2).

The Ts sequence may be up to 2.8 km thick if the generally northerly-dipping deposits observed in the Heelfly Creek quadrangle are a continuous, unfaulted sequence (Dee et al., 2015).

Cenozoic and Cretaceous Igneous Rocks

Igneous designations and naming conventions mostly from adjacent mapped geologic quadrangles, such as Dee et al. (2015) and McGrew (2018). Much of the metamorphosed Neoproterozoic and Paleozoic sedimentary rock units are pervasively intruded by Tmg, Tqd, and TKlg, and polygons of individual igneous rocks were mapped when the bodies were large enough to separate and differentiate from the intruded paragneiss unit.

Tb Aphyric basaltic dikes (middle Miocene) Dark gray-black, undeformed, nonfoliated, microcrystalline tholeiitic basalt to basaltic andesite. SiO_2 in two geochemical analyses were 48% and 58% (table 3), which may reflect variable differentiation. Observed as subvertical north-striking dikes, ≤1 m wide, discordantly crosscutting adjacent units including mylonitic foliations. Local chilled margins and commonly poorly exposed. Subcrop cannot be traced for more than 50 m along strike. Based on similarities to basalt dikes dated via $^{40}Ar/^{39}Ar$ dating in the Heelfly Creek quadrangle to the west and near Angle Lake to the northeast, probable ages span ca. 15 Ma to 17 Ma (C. Henry personal communication, 2020; Dee et al., 2015) (table 2). Snoke (1980) reported a ca. 17 Ma K-Ar age from a basalt dike around Dorsey Creek, near the southern extent of the Tent Mountain quadrangle.

Trcp Coarsely porphyritic rhyolite [Jarbidge-type rhyolite] (Miocene) Gray to pinkish-gray coarsely porphyritic rhyolite lavas that contain 25–30% phenocrysts of distinctive smoky quartz, sanidine, plagioclase, clinopyroxene, and generally altered mafic rocks that could be orthopyroxene or fayalite (Fe-rich olivine). Phenocrysts are commonly 6 mm and up to 12 mm in diameter. Phenocryst phases are rounded and embayed, with pockets of matrix in the phenocrysts. Plagioclase is faintly albite-twinned to more strongly grid-twinned, which suggests either anorthoclase or microcline. Similar grid-twinned feldspar occupies pockets in sanidine, and glomerocrysts of sanidine, grid-twinned feldspar, clinopyroxene, and opaque minerals (Fe-Ti oxides) occur in both rock types. Clinopyroxene has reaction rims with matrix. Microlites of feldspar laths are common in the glassy matrix of vitrophyres. Chemical analyses from the Heelfly Creek quadrangle show the rocks are Fe-rich rhyolites with ~75–76% SiO^2 (Dee et al., 2015).

Coarsely porphyritic Trcp contrasts to the finely porphyritic rhyolite lave (Trfp) exposed outside of the map area in the southern half of the Tent Mountain quadrangle. Trfp comprise Qmslrfp landslide blocks. There are two main exposures of Trcp in the northern half of the Tent Mountain quadrangle. In Deering Creek, in the northern map area, exposures are rarely flow banded, interbedded with Ts and up to ~30 m thick. The other major outcrop in the western map area consists of a prominent rhyolite cliff band, up to 50 m thick, with an irregularly exposed, black basal vitrophyre as much as 4 m thick overlain by massive to strongly flow-banded and locally columnar-jointed devitrified rock, and forms a resistant ledge that crops out for about 2 km.

The rhyolites are the southwesternmost known occurrences of Jarbidge-type rhyolites, which have the same distinctive phenocrysts and chemical characteristics (Coats, 1987; Brueseke et al., 2014). Jarbidge Rhyolite is most extensive near Jarbidge, NV, near the Idaho border where individual flows are more than 200 m thick, cumulative sections are at least 480 m thick, and total volume is estimated to be 500 km3 (Brueske et al., 2014). Similar Jarbidge-type rhyolites are present along the east side of the East Humboldt Range in the Welcome and Humboldt Peak quadrangles (McGrew and Snoke, 2015; McGrew, 2018).

New dating yielded $^{40}Ar/^{39}Ar$ anorthoclase ages of 15.33±0.01 Ma and 15.37±0.04 Ma for Trcp (southwestern Tent Mountain quadrangle) and Trfp (northwestern Secret Valley quadrangle, Snoke et al., in prep), respectively (table 2). These ages overlap other $^{40}Ar/^{39}Ar$ ages from Jarbidge-type rhyolites documented by Coats (1987) and Bruseke et al. (2014).

Tmg Biotite monzogranite orthogneiss (early Oligocene to middle Eocene) Moderately to strongly foliated, moderately to strongly lineated, medium-grained, equigranular biotite monzogranite and lesser tonalite and granodiorite (Batum, 1999). Geochemical analyses were ~65–75% SiO_2 (table 3). Protomylonitic fabrics indicate west- to northwest-directed shear. Rare asymmetric folds of intra-Tmg leucosome layers suggest top-east shear, possibly from earlier pre-mylonitic history. Contains approximately 10% biotite and subequal proportions of oligoclase, alkali feldspar, and quartz. Commonly forms tabular sheets that are concordant to slightly discordant, up to 70 m thick but typically 1–10 m. Forms prominent blocky dark gray to dark brown cliffs. New U-Pb zircon dating in this study yielded an age of ca. 31.5 Ma from 18 concordant analyses (fig. 3; table 4), consistent with older U-Th-Pb zircon and monazite ages from Lamoille Canyon in the Ruby Mountains of 29 ± 0.5 Ma (Wright and Snoke, 1993).

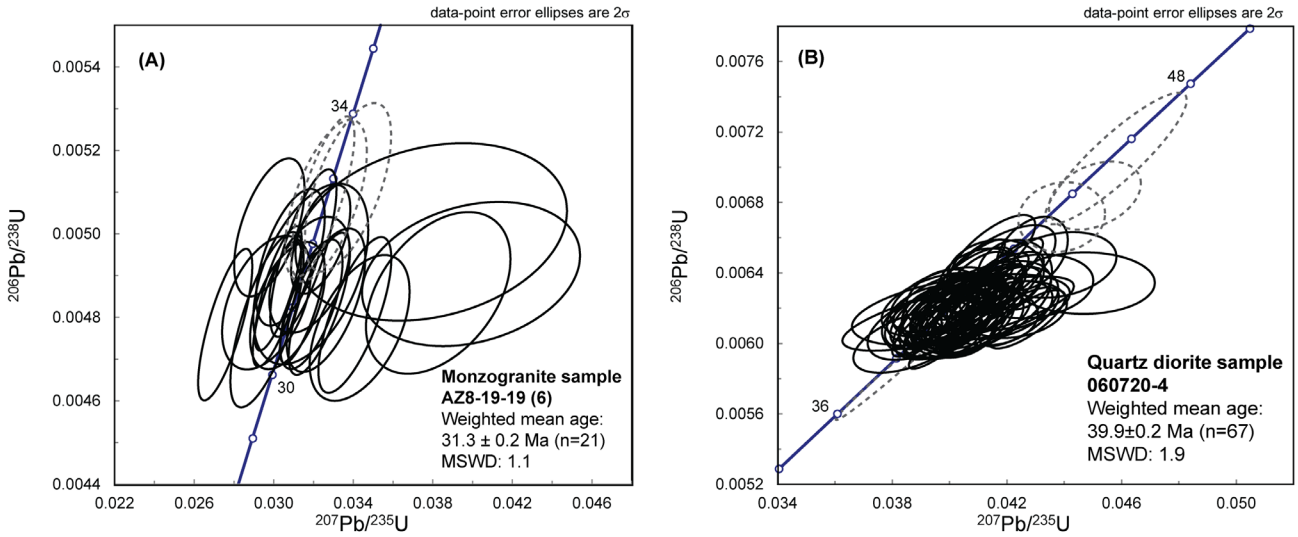

Figure 3. U-Pb concordia diagrams showing results of zircon analyses of (A) monzogranite sample AZ8-19-19(6) and (B) quartz diorite sample 060720-4. Solid ellipses were analyses used in the weighted mean calculation and dashed ellipses were excluded because they fell outside of the dominant age population. Isoptopic data in tables 4 and 5.

Tqd Hornblende-biotite quartz dioritic orthogneiss (middle Eocene) Weakly to strongly foliated, weakly to strongly lineated, porphyritic appearance with 1–2 mm plagioclase, with lesser hornblende, biotite, and quartz. Conspicuously less foliated, lineated, and sheared than adjacent metamorphosed rocks, possibly due to its greater strength than the other units. Geochemical analyses show ~60–65% SiO_2 (table 3). Forms dark gray-black, jagged, high-relief cliffs that commonly define ridges. Mostly subparallel to dominant foliation, but also discordant to oblique to primary foliation. Intermingled with TKlg, and crosscut by Tmg and a late undeformed TKlg. Ridges and dip slopes commonly consist of intermingled Tqd and lesser TKlg. In Tent Mountain, intrusions concentrate in O€mi, close to the contact with the underlying €Zpmi paragneiss. Defines the major north-trending ridgeline of Hole in the Mountain Peak, separating Lizzies Basin on the east from the Boulder Creek drainages on the west. Previously dated in the Humboldt Peak quadrangle at ca. 40 Ma by U-Pb zircon ID-TIMS (Wright and Snoke, 1993) and SHRIMP (Premo et al., 2014). New U-Pb zircon dating in this study yielded an age of 39.9±0.2 Ma from 67 concordant analyses (fig. 3; table 5).

TKlg Leucogranite and leucogranitic orthogneiss (Oligocene to Cretaceous) Weakly to strongly foliated, coarse to medium grained, commonly pegmatitic, leucogranite. Includes lesser trondhjemitic pegmatite, muscovite-rich two-mica leucogranite, and weakly foliated, fine-to medium-grained late-stage garnet aplite dikes (Batum, 1999). Mylonitic fabrics indicate west-to northwest-directed shear. Foliated leucogranite commonly forms discontinuous meter to sub-meter scale concordant sheets, pods or lenses throughout the rocks in the metamorphic core complex. Mappable lenses of Tklg are up to 50 m thick. Structurally deeper leucogranite bodies in the northeastern-eastern map area are commonly surrounded by restitic biotite-sillimanite schist. Weakly foliated aplite dikes cut foliation. A leucogranite in the Welcome quadrangle to the northeast yielded a 207Pb/206Pb zircon date of 85 ± 3 Ma (McGrew and Snoke, 2015), similar to leucogranite ages from the southern East Humboldt Range and Ruby Mountains (Snoke et al., 1990). Hallett and Spear (2015) presented ca. 80 Ma U-Pb monazite ages from leucosome sampled from the Winchell Lake nappe in the Humboldt Peak quadrangle.

Most leucogranite is interpreted to be Late Cretaceous (Wright and Snoke, 1993; McGrew et al., 2000), but observations of TKlg intermingled with, or directly cross cutting, the Cenozoic Tqd and Tmg intrusions require that the TKlg age range extends to as young as Oligocene (e.g., McGrew, 2018).

Paleozoic Sedimentary Rocks

Mc Conglomerate and shale (Mississippian) Brown siliclastic unit, mostly consisting of unmetamorphosed pebble conglomerate and shale, with limited exposure in the northern part of the map area adjacent to Ackler Creek. Pebble grains are white-gray and dark black centimeter-scale clasts of quartzite and chert. Unit is interpreted to correlate with either the Mississippian Chainman Shale or Diamond Peak Formation.

Metamorphosed Paleozoic and Neoproterozoic Sedimentary Rocks

This map uses the stratigraphic framework established by Hurlow (1987)'s mapping of the southern portion of the Tent Mountain quadrangle. Unit designations and naming convention follow McGrew and Snoke (2015), Dee and

Ressel (2016), and McGrew (2018). Most rocks are strongly foliated, lineated, and mylonitized showing west- to northwest-directed shear. The structurally deepest samples in the valley bottoms of the central map area appear less strained, lineated, mylonitized, and sheared, possibly due to depth below the main mylonitic shear front. Mesozoic-Cenozoic sills and dikes intrude most of these units, commonly making up 1/2 to >2/3 of the rock exposure. Mapping focused on dividing prominent metasedimentary host-rock lithology.

M€sq Schist and quartzite paragneiss (Mississippian to Cambrian) Dark rust gray to brown micaceous feldspathic quartzite and metaconglomerate, quartzofeldspathic schist, pelitic schist, and minor calcareous paragneiss, previously mapped as the "metaclastic" unit by Hurlow (1987), who correlated it with Mississippian siliciclastic rocks. Minor calc-silicate and calcareous paragneiss comprise the lower part of the unit. Unit appears similar to the MDgs unit mapped in the Winchell Lake nappe in the Humboldt Peak quadrangle to the east (McGrew, 2018). The extensive siliciclastic rocks, especially the fine-grained quartzite and schist, are distinct from the McCoy Creek Group rocks, leading to its correlation with Paleozoic rocks.

The unit is found in the west of the map area, where it is juxtaposed between probable Cambrian marbles and Cambrian-Neoproterozoic Prospect Mountain-McCoy Creek paragneiss (€Zpmi). It most likely correlates with one of two Paleozoic siliciclastic sections. It may represent Mississippian Diamond Peak Formation and Chainmain Shale, with the lower calcareous paragneiss correlating with Mississippian Joana or Tripon Pass Limestones. Its rust brown appearance and the presence of highly strained metaconglomerate support this interpretation. This correlation requires complex infolding, unit duplication and excision, or another complicated structural history. One permissible history involves earlier thrusting of Paleozoic strata over M€qs, and during extensional shear, M€qs was juxtaposed directly over €Zpmi. This interpretation is not unique.

Alternatively, the unit may represent siliciclastic Cambrian units, from the Morgan Pass Formation to Dunderburg Shale, which also includes numerous silty marbles. This interpretation implies that M€qs is in the correct stratigraphic and structural position, and thus does not require complex structural features. Future analyses are needed to better correlate this unit.

M€mu Marble, undivided (Mississippian to Cambrian) Undivided white to blue limestone marble, dolomite marble with sparse graphite and tremolite.

Dg Guilmette Formation (Devonian) Fine-grained blue-gray to white calcite marble with white color bands, recrystallized fossils, and graphite. Some dolomite layers. In contact with O€mi, without intervening Oe, suggests normal-sense structural omission.

DOd Dolomite and marble (Devonian to Ordovician) White to blue-gray, fine-grained, massive dolomite marble with sparse graphite and tremolite. Subordinate marbles interbedded with mostly dolomite. Distinguished from M€mu by abundance of dolomite.

Oe Metamorphosed Eureka Quartzite (Ordovician) Finely recrystallized mylonitized white quartzite with foliation defined by minor muscovite and graphite bands. Outcrops as lag deposits over lower Paleozoic marbles or in a cliff face with ~3 m thickness in the western map area. Quartz grains are flattened and stretched, and show evidence for bulging, and lesser subgrain rotation, recrystallization. Recrystallized grain size is ~6 µm, and c-axis pole figures from quartz grains suggest a mix of basal, rhomb, and prism <a> slip activity. These observations broadly support deformation at approximate temperatures in the range of ~400°C and relatively high flow stress conditions, consistent with Oe deforming at a structurally higher, colder, and stronger part of the mylonitic shear zone compared with €Zpm and €Zpmi quartzites.

O€m Impure calcite marble (Ordovician to Cambrian) Variably impure calcite, dolomite, and calc-silicate marble with variable amounts of tan-to-orange silty interbeds. Marbles have heterogenous color and appearance, including pale white-gray coarse-grained massive layers, fine-grained gray-blue banded layers, green-gray to gray impure silty marble, and coarse massive blue-gray layers. Commonly muscovite-rich with graphite and tremolite. Calc-silicate with diopside and garnet observed along margins when unit is intruded by TKlg and Tqd. Lowermost part of unit includes highly folded siliciclastic and impure marble layers.

Contact with the underlying €Zpm or €Zpmi is sharp, marked by the presence of pure quartzite beds and disappearance of marbles. Some marbles near, or below, this interpreted contact may be Zmm marbles, which are commonly thinner (mostly <5 m thick) and surrounded by quartzite and pelite.

O€mi Intruded impure calcite marble (Ordovician to Cambrian) Similar host-rock lithology of O€m, except extensively intruded by leucogranite, quartz diorite, and monzogranite. Lecuogranite, granite, and quartz diorite commonly boudinaged within intruded layers and isolated igneous boudins observed in flowing limestone marbles. In the Hole in the Mountain cirque headwall, the unit is bleached tan-white with less color variation than elsewhere in the map area.

€Zpm Metamorphosed Prospect Mountain Quartzite (Cambrian to Neoproterozoic) and McCoy Creek Group (Neoproterozoic) Micaceous feldspathic quartzite with subordinate pelitic schist, and locally with calc-silicate gneiss and rare para-amphibolite. Upper unit commonly consists of a relatively pure quartzite interpreted to correlate with the Prospect Mountain Quartzite. Rare intrusions compared with mapped €Zpmi.

€Zpmi Intruded metamorphosed Prospect Mountain Quartzite (Cambrian to Neoproterozoic) and McCoy Creek Group (Neoproterozoic) Similar host-rock lithology of €Zpm, except extensively intruded by leucogranite, quartz diorite, and monzogranite. Commonly migmatitic, with pelitic rocks hosting a higher percentage of leucosome than quartzitic rocks. Leucosome occurs in centimeter-scale to meter-scale concordant pods, sheets, and lenses commonly bordered by biotite-sillimanite resistic schist. Pelitic schist consists of the metamorphic mineral assemblage of biotite, sillimanite, and garnet, and titanite (e.g., McGrew et al., 2000; Hallett and Spear, 2014).

Quartz textures display interlobate grain boundaries and smaller grains tend to be equigranular and polygonalized. This reflects a mix of grain boundary migration and subgrain rotation recrystallization. Recrystallized grain size range from 30–50 µm across the study area. C-axis pole figures from quartz grains suggest dominantly prism <a> slip activity with lesser rhomb <a>. Together, these observations support deformation at very approximate temperatures in the range of ~500°C and moderate flow stress conditions, consistent with these rocks deforming at structurally lower, hotter, and weaker parts of the mylonitic shear zone compared with Oe in the western part of the map area.

Zmu Metamophosed McMcoy Creek Group, undivided (Neoproterozoic) Micaceous quartzite, feldspathic quartzite, garnet-biotite schist (±sillimanite) with lesser marble, calc-silicate, and rare amphibolite. Extensively intruded by leucogranite, monzogranite, and quartz diorite. Divided from €Zpmi or €Zpm based on occurrence of extensive pelitic layers or interlayered coarse white-gray Zmm marbles.

The lower structural levels of this unit are likely correlative with the paragneiss of Greys Peak (McGrew and Snoke, 2015; McGrew, 2018). In the northeastern most part of the map area, a thin pure white quartzite surrounded by micaceous feldspathic quartzite and biotite schist is interpreted to be similar to the paragneiss of Greys Peak as described by McGrew (2018) in the Humboldt Peak quadrangle to the east.

Zmm McMcoy Creek Group marble (Neoproterozoic) Discontinuous coarse-grained graphite-bearing white-gray calcite marble. Forms continuous and discontinuous layers that range in thickness from ~1 m to ~100 m (mostly <5 m). Marble margins are sometimes replaced by calc-silicate assemblages with diopside, grossular garnet, and actinolite. Divided from O€m and O€mi because Zmm layers are commonly thin, always white-gray in color, and surrounded by quartzite and pelite.

ACKNOWLEDGMENTS

Research supported by the U.S. Geological Survey, National Cooperative Geologic Mapping Program, under USGS award number G19AC00383. The views and conclusions contained in this document are those of the authors and should not be interpreted as necessarily representing the official policies, either expressed or implied, of the U.S. Government. We thank Drew Levy and Chris Henry for field assistance, analyses of some samples, and discussions of the geology.

REFERENCES

Balco, G., Stone, J.O., Lifton, N.A., and Dunai, T.J., 2008, A complete and easily accessible means of calculating surface exposure ages or erosion rates from ^{10}Be and ^{26}Al measurements: Quaternary geochronology, v. 3, no. 3, p. 174–195.

Batum, M.A., 1999, Petrology of Late Cretaceous and Cenozoicgranitic rocks, East Humboldt Range: Texas Tech University, Lubbock, M.S Thesis, 167 p.

Brueseke, M.E., Callicoat, J.S., Hames, W., and Larson, P.B., 2014, Mid-Miocene rhyolite volcanism in northeastern Nevada—the Jarbidge Rhyolite and its relationship to the Cenozoic evolution of the northern Great Basin (USA): Geological Society of America Bulletin, v. 126, p. 1047–1067.

Coats, R.R., 1987, Geology of Elko County, Nevada: Nevada Bureau of Mines and Geology Bulletin, 101, 112 p.

Dee, S., and Ressel, M.W., 2016, Preliminary geologic map of the Herder Creek quadrangle, Elko County, Nevada: Nevada Bureau of Mines and Geology Open-File Report 16-5, scale 1:24,000, 5 p.

Dee, S., Dering, G.M., and Henry, C.D., 2015, Preliminary geologic map of the Heelfly Creek quadrangle and adjacent parts of the Tent Mountain, Soldier Peak, and Secret Valley quadrangles, Elko County, Nevada: Nevada Bureau of Mines and Geology Open-File Report 15-4, scale 1:24,000, 5 p.

Gehrels, G.E., Valencia, V.A., and Ruiz, J., 2008, Enhanced precision, accuracy, efficiency, and spatial resolution of U-Pb ages by laser ablation–multicollector–inductively coupled plasma–mass spectrometry: Geochemistry, Geophysics, Geosystems, v. 9.

Hallett, B.W., and Spear, F.S., 2014, The P–T history of anatectic pelites of the Northern East Humboldt Range, Nevada—evidence for tectonic loading, decompression, and anataxis: Journal of Petrology, v. 55, p. 3–36.

Hallett, B.W., and Spear, F.S., 2015, Monazite, zircon, and garnet growth in migmatitic pelites as a record of metamorphism and partial melting in the East Humboldt Range, Nevada: American Mineralogist, v. 100, p. 951–972.

Hurlow, H.A., 1987, Structural geometry, fabric, and chronology of a Tertiary extensional shear zone-detachment system, southwestern East Humboldt Range, Elko County, Nevada: University of Wyoming, Laramie, M.S. thesis, 141 p.

Laabs, B.J.C., Licciardi, J.M., Leonard, E.M., Munroe, J.S., and Marchetti, D.W., 2020, Updated cosmogenic chronologies of Pleistocene mountain glaciation in the western United States and associated paleoclimate inferences: Quaternary Science Reviews, v. 242, p.1–36.

Ludwig, K., 2008, Isoplot version 4.15—a geochronological toolkit for Microsoft Excel: Berkeley Geochronology Center, Special Publication, 76p.

McGrew, A., 2018, Geologic map of the Humboldt Peak quadrangle, Elko County, Nevada: Nevada Bureau of Mines and Geology Map 186, scale 1:24,000, 23 p.

McGrew, A.J., and Snoke, A.W., 2015, Geologic map of the Welcome and adjacent part of the Wells quadrangle, Elko County, Nevada: Nevada Bureau of Mines and Geology Map 184, scale 1:24,000, inset 1:12,000, p. 40.

McGrew, A.J., Peters, M.T., and Wright, J.E., 2000, Thermobarometric constraints on the tectonothermal evolution of the East Humboldt Range metamorphic core complex, Nevada: Geological Society of America Bulletin, v. 112, p. 45–60.

McKinney, S.T., Cottle, J.M., and Lederer, G.W., 2015, Evaluating rare earth element (REE) mineralization mechanisms in Proterozoic gneiss, Music Valley, California: Geological Society of America Bulletin, v. 127, p. 1135–1152.

Middlemost, E.A., 1994, Naming materials in the magma/igneous rock system: Earth-Science Reviews, v. 37, p. 215–224.

Paton, C., Woodhead, J.D., Hellstrom, J.C., Hergt, J.M., Greig, A., and Maas, R., 2010, Improved laser ablation U-Pb zircon geochronology through robust downhole fractionation correction: Geochemistry, Geophysics, Geosystems, v. 11, p. 1–36.

Premo, W.R., Moscati, R.J., McGrew, A.J., and Snoke, A.W., 2014, New U-Pb zircon geochronology of Precambrian paragneisses and late Phanerozoic orthogneisses of the Angel Lake-Lizzie Basin region of the East Humboldt Range, northeastern Nevada—a comparison with the thermal chronology at Lamoille Canyon in the adjacent Ruby Mountains: Geological Society of America Abstracts with Programs, v. 46, p. 33.

Sharp, R.P., 1938, Pleistocene glaciation in the Ruby-East Humboldt Range, northeastern Nevada: Journal of Geomorphology, v. 1, p. 296–323.

Sharp, R.P., 1940, Geomorphology of the Ruby-East Humboldt Range, Nevada: Bulletin of the Geological Society of America, v. 51, no. 3, p. 337–371.

Snoke, A.W., 1980, Transition from infrastructure to suprastructure in the northern Ruby Mountains, Nevada, *in* Crittenden, M.D., Jr., Coney, P.J., and Davis, G.H., editors, Cordilleran metamorphic core complexes: Boulder, Colorado, Geological Society of America Memoir 153, p. 287–333.

Snoke, A.W., McGrew, A.J., Valasek, P.A., and Smithson, S.B., 1990, A crustal cross section for a terrain of superimposed shortening and extension—Ruby Mountains-East Humboldt Range metamorphic core complex, Nevada, *in* Salisbury, M.H., and Fountain, D.M., editors, Exposed cross sections of the continental crust: Dordrecht, The Netherlands, Kluwer Academic Publishers, p. 103–135

Snoke, A.W., Howard, K.A., and Dee, S., in prep, Geologic map of the Secret Valley quadrangle, Elko County, Nevada: Nevada Bureau of Mines and Geology Map 189, scale 1:24,000, 20 p.

Stacey, J.S., and Kramers, J.D., 1975, Approximation of terrestrial lead isotope evolution by a two-stage model: Earth and Planetary Science Letters, v. 26, p. 207–221.

Wesnousky, S.G., and Willoughby, C.H., 2003, Neotectonic note—the Ruby–East Humboldt Range, northeastern Nevada: Seismological Society of America Bulletin, v. 93, no. 3, p. 1345–1354.

Wright, J.E., and Snoke, A.W., 1993, Tertiary magmatism and mylonitization in the Ruby-East Humboldt metamorphic core complex, northeastern Nevada—U-Pb geochronology and Sr, Nd, and Pb isotope geochemistry. Bulletin of the Geological Society of America, v. 105, p. 935–952.

Suggested citation:

Zuza, A.V., Dee, S., and Laabs, B.J.C., 2020, Geologic map of the north half of the Tent Mountain quadrangle, Elko County, Nevada: Nevada Bureau of Mines and Geology Open-File Report 20-3, scale 1:24,000, 16 p.

© Copyright 2020 The University of Nevada, Reno. All Rights Reserved.

Table 1. Cosmogenic ^{10}Be exposure ages of boulders atop Qgo surfaces at Boulder Creek and Greys Creek

Drainage	Map unit	Sample	Zero-erosion exposure age (ka)	Internal uncertainty (kyr)	External uncertainty (kyr)	1 mm-kyr-erosion exposure age (ka)	Internal uncertainty (kyr)	External uncertainty (kyr)	7.5' quadrangle	Lat83	Long83	Elevation (m asl)	Topographic shielding	Nuclide concentration (atoms ^{10}Be/g SiO_2)	Uncertainty (atoms ^{10}Be/g SiO_2)
Greys Creek	Qgo_1	GC16-08	70.8	1.5	3.1	75.5	1.7	3.5	Herder Creek	41.05799	-115.15191	1893	0.9957	1.27E+06	2.68E+04
Greys Creek	Qgo_1	GC16-09	22.2	1.4	1.6	22.6	1.4	1.7	Herder Creek	41.05789	-115.15218	1892	0.9957	3.96E+05	2.41E+04
Greys Creek	Qgo_1	GC16-10	14.6	0.6	0.8	14.7	0.6	0.8	Herder Creek	41.05789	-115.15250	1887	0.9957	2.50E+05	1.04E+04
Greys Creek	Qgo_1	GC16-11	69.7	3.3	4.3	74.4	3.8	4.9	Herder Creek	41.05813	-115.15375	1869	0.9958	1.23E+06	5.79E+04
Greys Creek	Qgo_1	GC16-12	72.2	1.9	3.4	77.1	2.2	3.8	Herder Creek	41.05831	-115.15426	1867	0.9958	1.27E+06	3.29E+04
Greys Creek	Qgo_1	GC16-13	23.5	1	1.3	23.9	1	1.4	Herder Creek	41.05846	-115.15647	1841	0.9779	3.98E+05	1.65E+04
Greys Creek	Qgo_1	GC16-14	24.9	0.8	1.2	25.4	0.8	1.2	Herder Creek	41.05850	-115.15639	1841	0.9958	4.32E+05	1.36E+04
Greys Creek	Qgo_2	GC16-01	135	10	11	154	13	15	Herder Creek	41.06001	-115.15404	1848	0.9962	2.38E+06	1.71E+05
Greys Creek	Qgo_2	GC16-02	97.1	2.4	4.5	105	3	5	Herder Creek	41.06077	-115.15296	1848	0.9962	1.69E+06	4.13E+04
Greys Creek	Qgo_2	GC16-03	152	3.4	6.9	177	5	9	Herder Creek	41.06141	-115.15246	1846	0.9962	2.67E+06	5.81E+04
Greys Creek	Qgo_2	GC16-04	142	10	12	163	14	16	Herder Creek	41.06119	-115.15239	1848	0.9962	2.50E+06	1.78E+05
Greys Creek	Qgo_2	GC16-05	101	4.4	5.9	110	5	7	Herder Creek	41.05909	-115.15170	1887	0.9957	1.82E+06	7.69E+04
Greys Creek	Qgo_2	GC16-06	161	8.9	11	188	12	15	Herder Creek	41.05886	-115.15088	1897	0.9957	2.93E+06	1.55E+05
Greys Creek	Qgo_2	GC16-07	165	4.5	7.9	193	6	11	Herder Creek	41.05882	-115.15155	1893	0.9957	2.99E+06	7.89E+04
Boulder Creek	Qgo_2	BC16-01	126	2.9	5.7	143	4	7	Tent Mountain	40.97158	-115.24112	1800	0.9998	2.16E+06	4.76E+04
Boulder Creek	Qgo_2	BC16-02	25.6	0.9	1.3	26.1	0.9	1.4	Tent Mountain	40.97160	-115.24073	1802	0.9901	4.29E+05	1.43E+04
Boulder Creek	Qgo_2	BC16-03	130	3.3	6	147	4.3	7.8	Tent Mountain	40.97190	-115.24128	1797	0.9998	2.21E+06	5.47E+04
Boulder Creek	Qgo_2	BC16-04	24	0.7	1.2	24.5	0.8	1.2	Tent Mountain	40.97132	-115.23992	1807	0.9998	4.05E+05	1.24E+04
Boulder Creek	Qg_{o2}	BC16-05	129	2.5	5.6	146	3	7	Tent Mountain	40.97160	-115.24148	1798	0.9986	2.19E+06	4.14E+04
Boulder Creek	Qgo_2	BC16-06	45.9	3.9	4.3	48.4	4.3	4.7	Tent Mountain	40.97144	-115.24208	1796	0.9998	7.85E+05	6.60E+04
Boulder Creek	Qgo_2	BC16-07	58.4	2.3	3.2	62.2	2.5	3.6	Tent Mountain	40.96729	-115.23989	1809	0.9996	9.74E+05	3.80E+04
Boulder Creek	Qgo_2	BC16-08	29.1	0.9	1.4	29.8	1	1.5	Tent Mountain	40.96937	-115.24137	1804	0.9998	4.95E+05	1.56E+04

Note: ages are computed with the Version 3.0 exposure age calculator formerly known as the CRONUS-Earth online calculator (Balco et al., 2008; http://hess.ess.washington.edu). Ages are based on a regionally calibrated production rate from Promontory Point, Utah, scaled for elevation, latitude, and time using the "LSDn" scheme. For all age calculations, the elevation/pressure relationship defined by the ERA-40 analysis (coded "std" in the Version 3 calculator) is assumed along with a sample density of 2.7 g/cm3. All samples were collected in year 2016, and beryllium-10 was extracted from quartz separated from rock samples sawn to a thickness of 1.5 cm. Erosion rates are unknown and likely vary between lithologies, estimated rates of zero and 1 mm/kyr were used to compute exposure ages shown in table 1. Beryllium-10 ratios were measured by accelerator mass spectrometry against a standard coded "KNSTD07" in the Version 3 calculator.

Table 2. Summary of $^{40}Ar/^{39}Ar$ ages of Cenozoic igneous rocks in and around the Tent Mountain quadrangle (mostly single-crystal analyses except H14-55)

Sample	Rock type	Map Unit	Analyzed phase	Ag (Ma)	2σ	K/Ca	2σ	n/nt*	Quadrangle	Elev. (m)	Lat83	Long83	Source	Note
H14-52	rhyolite lava	Trcp	anorthoclase	15.33	0.01	9.6	5.2	16/21	Tent Mountain	1938	40.951696	-115.247157	Unpublished; C. Henry	
GD14-116B	tephra in Ts	Ts	anorthoclase	15.77	0.02	6	4.6	15/20	Tent Mountain	1868	40.951838	-115.249631	Unpublished; C. Henry	
H14-55	mafic dike	Tb	matrix	16.85	0.10	0.39	0.08	-	Tent Mountain	2121	40.884311	-115.238766	Unpublished; C. Henry	step-heated sample; 50.3 %^{39}Ar for reported age
H14-54	rhyolite lava	Trfp	anorthoclase	15.37	0.04	9	1.9	24/25	Secret Valley	1984	40.869185	-115.246145	Unpublished; C. Henry	
H14-97	tephra in Ts	Ts	sanidine	<22.89	0.01	62.5	3.3	4/20	Heelfly Creek	1803	40.886682	-115.300108	Unpublished; C. Henry	maximum age; young population of 4
H14-98	tephra in Ts	Ts	sanidine	<22.7	0.30	0	0	3/12	Heelfly Creek	1798	40.885471	-115.29859	Unpublished; C. Henry	maximum age; young population of 3
GD14-100	tephra in Ts	Ts	anorthoclase	8.3	0.20	8.5	7.8	11/19	Heelfly Creek	1805	40.912628	-115.291149	Unpublished; C. Henry	
GD14-113	tephra in Ts	Ts	plagioclase	10.3	0.13	0.2	0	15/19	Heelfly Creek	1825	40.946898	-115.265256	Unpublished; C. Henry	
H15-43	tephra in Ts	Ts	detrital feldspar	5.15	1.82	0.1	0.1	6/23	Herder Creek	1835	41.01018	-115.21594	Dee and Ressel (2016)	maximum age; population of 6
H15-42	reworked tephra in Ts	Ts	detrital feldspar	<23.27	0.02	20.5	-	1/24	Herder Creek	1772	41.00875	-115.21871	Dee and Ressel (2016)	maximum age; single youngest analysis reported; ~63% of analyses spanned ca. 30 to 23 Ma

n/nt* -- number of analyses used in calculated age over the total number of analyses

Table 3. Geochemical data from Tent Mountain and adjacent Humboldt Peak quadrangles

Sample	AZ7-30-20(1)	AZ6-29-20(1)	070720-2	080720-3	080720-4	080720-7	090720-10	090720-4	090720-8	100720-6
Unit	Tb	Tb	TKlg	TKlg	TKlg	TKlg	TKlg	TKlg	TKlg	TKlg
Latitude	40.976278	40.956738	40.941621	40.914112	40.914112	40.915892	40.91116	40.91076	40.90635	40.847527
Longitude	-115.159368	-115.212236	-115.21617	-115.1099	-115.10985	-115.11345	-115.13024	-115.11533	-115.12651	-115.08707
Major and Minor Elements (%)										
SiO_2	44.70	56.80	77.60	76.70	77.50	75.60	75.80	74.90	74.90	80.00
Al2O3	14.75	18.00	13.60	14.55	13.75	13.95	14.65	14.45	14.60	12.30
FeO*	9.93	6.92	0.69	0.78	0.72	0.59	0.79	1.86	0.78	0.49
CaO	8.44	6.92	1.21	0.44	0.89	0.86	0.63	1.56	2.42	1.34
MgO	6.06	3.29	0.14	0.06	0.02	0.07	0.04	0.38	0.17	0.09
Na2O	3.43	3.40	3.42	4.22	4.35	3.43	4.49	3.89	3.45	2.89
K2O	2.88	1.76	4.31	3.86	3.66	4.82	4.71	2.83	3.67	3.48
Cr2O3	0.02	0.00	0.01	0.00	0.00	0.00	0.00	0.00	0.00	0.00
TiO2	2.29	1.10	0.07	0.02	0.02	0.04	0.01	0.26	0.06	0.04
MnO	0.17	0.11	0.01	0.08	0.02	0.01	0.03	0.02	0.01	0.01
P2O5	0.74	0.22	0.03	0.15	0.03	0.04	0.13	0.06	0.03	0.08
SrO	0.11	0.04	0.00	0.00	0.00	0.00	0.00	0.02	0.02	0.02
BaO	0.14	0.09	0.03	0.01	0.01	0.02	0.02	0.11	0.07	0.08
LOI	4.97	0.96	0.55	0.62	0.31	0.51	0.32	0.74	0.29	0.56
Total	93.66	98.65	101.12	100.87	100.97	99.43	101.30	100.34	100.18	100.82
Trace Elements (ppm)										
Ba	1285	721	277	54	71.2	179	180	963	569	703
Ce	97.1	55.8	12.6	4.2	27.1	7.9	3.1	178.5	9.3	11
Cr	120	10	30	10	10	10	10	10	10	10
Cs	7.42	2.95	0.92	3.67	1.97	1.2	3.63	0.82	1.07	0.39
Dy	6.15	4.46	2.14	1.53	13.9	2.56	0.37	5.41	1.84	0.87
Er	2.75	2.35	1.68	0.6	8.82	1.81	0.15	1.06	1.15	0.54
Eu	2.56	1.41	0.41	0.06	0.32	0.21	0.04	1.3	0.47	0.89
Ga	22.8	22.5	18.4	24.8	21.8	20.5	24.9	22.2	21.8	13.3
Gd	7.79	4.64	1.69	1.11	8.3	1.63	0.49	12	1.28	0.99
Hf	6.6	4.6	6	1.4	1	1	1.6	3	1.6	0.4
Ho	1.07	0.89	0.52	0.26	2.8	0.58	0.06	0.68	0.37	0.18
La	52.6	28.3	6.9	2	13.6	4.6	1.1	95.2	5.1	6.5
Lu	0.37	0.37	0.34	0.12	1.69	0.35	0.03	0.08	0.19	0.07
Nb	86.5	11.1	11.9	28.7	17.2	11.7	90.7	14.3	7.4	1.6
Nd	45.3	25	5.6	1.9	12.8	3.2	1.4	73.5	3.8	4.7
Pr	11.1	6.4	1.41	0.49	3.11	0.87	0.39	20	1.04	1.24
Rb	86.7	60.6	184	311	249	180	291	99.8	133.5	69.6
Sm	8.89	5.11	1.36	1.04	5.17	0.97	0.64	15.4	1.11	1.05
Sn	2	1	1	10	4	2	3	1	1	1
Sr	984	436	75.9	25.1	28.6	83.9	54.3	283	239	242
Ta	4.8	0.8	1.1	4.8	3.4	2	30.6	0.9	1.5	0.3
Tb	1.1	0.7	0.31	0.26	1.9	0.4	0.08	1.4	0.28	0.17
Th	7.65	8.05	29.1	2.29	37	5.09	2.23	42.9	6.54	2.15
Tm	0.43	0.31	0.29	0.12	1.5	0.3	0.02	0.09	0.17	0.08
U	1.8	1.57	4.25	5.23	27.2	11.05	5.1	7.7	8.02	0.4
V	192	161	6	<5	<5	<5	<5	10	5	<5
W	2	1	2	3	1	2	4	1	2	1
Y	29.2	22.1	15.3	8.1	86.2	18.1	1.9	16.4	11.8	5.6
Yb	2.5	2.21	2.05	0.89	10.55	2.08	0.17	0.5	1.21	0.43
Zr	303	174	107	26	26	19	18	109	37	15

Table 3. Geochemical data from Tent Mountain and adjacent Humboldt Peak quadrangles (continued)

Sample	110720-13	110720-5	101019-11	100720-2	080720-2	080720-6	090720-12	AZ 7-8-20 (1b)	110720-1	AZ6-30-20(4)
Unit	TKlg	TKlg	Tmg	Tmg	Tmg	Tmg	Tmg	Tmg	Tmg	Tmg
Latitude	40.771935	40.769727	40.96659	40.8159	40.91411	40.91589	40.91291	40.91403	40.77265	40.94133
Longitude	-115.294041	-115.285812	-115.19	-115.12	-115.11	-115.1135	-115.1281	-115.1092	-115.306	-115.199
Major and Minor Elements (%)										
SiO2	74.90	75.10	72.20	73.10	67.90	75.40	74.10	73.50	70.90	76.80
Al2O3	13.50	14.85	14.35	14.40	17.60	13.75	13.40	13.55	14.50	12.95
FeO*	0.56	0.80	2.11	1.69	3.31	1.55	2.10	2.09	2.09	1.01
CaO	0.61	1.69	1.80	1.41	3.95	0.88	1.04	1.03	2.52	0.95
MgO	0.13	0.08	0.51	0.35	0.75	0.18	0.32	0.28	0.41	0.13
Na2O	2.32	4.98	3.36	3.38	4.64	3.33	3.00	2.78	3.79	3.39
K2O	6.90	1.71	4.19	4.38	1.29	4.94	4.68	5.32	2.41	4.60
Cr2O3	0.00	0.00	0.00	0.01	0.00	0.00	0.00	0.00	0.00	0.00
TiO2	0.04	0.01	0.29	0.21	0.36	0.13	0.23	0.17	0.20	0.07
MnO	0.01	0.03	0.05	0.04	0.04	0.03	0.03	0.03	0.04	0.02
P2O5	0.01	0.03	0.09	0.08	0.19	0.04	0.04	0.05	0.09	0.05
SrO	0.04	0.02	0.01	0.02	0.04	0.01	0.01	0.00	0.17	0.00
BaO	0.42	0.04	0.11	0.12	0.07	0.07	0.09	0.09	0.19	0.06
LOI	0.45	0.68	0.55	0.68	0.66	0.52	0.44	0.35	0.47	0.26
Total	99.44	99.34	99.07	99.19	100.14	100.31	99.04	98.89	97.31	100.03
Trace Elements (ppm)										
Ba	4180	353	1015	1125	557	637	744	840	1805	494
Ce	5.4	16.2	78.5	59.2	127	111	137.5	148	103.5	58
Cr	10	10	20	40	10	10	10	10	10	10
Cs	0.5	0.44	2.54	1.73	5.14	1.39	1.75	0.89	0.48	3.35
Dy	0.13	1.46	4.96	2.56	2.53	4.35	5.07	3.77	1.97	5.45
Er	0.07	0.95	2.7	1.3	1.11	1.67	2.54	1.53	1.03	2.76
Eu	0.97	1.29	0.88	0.74	1.5	0.68	0.68	0.72	1.38	0.41
Ga	12.8	14.2	22.4	21.7	22.1	20.9	20.2	19.4	21.6	23
Gd	0.26	1.28	5.16	3.07	4.25	6.58	6.94	6.38	3.77	4.88
Hf	0.4	0.5	5.4	3.8	8	5.1	6.4	5.9	4	3.9
Ho	0.02	0.34	1.02	0.5	0.47	0.7	0.93	0.64	0.36	1.07
La	3.2	8.6	43.2	34.9	73.7	62	74	79.4	55.3	29.6
Lu	0.01	0.18	0.39	0.21	0.13	0.2	0.38	0.17	0.12	0.38
Nb	2	0.6	25.7	14.7	8	19.6	18	14.8	6.2	20.6
Nd	1.8	6.8	30	22.6	43.9	39.1	50.1	52.4	42.2	22.2
Pr	0.54	1.85	8.39	6.34	12.75	11.5	14.6	15	11.4	6.45
Rb	159	28.9	164.5	157	105.5	209	203	215	71.2	272
Sm	0.35	1.71	5.49	4.05	6.36	7.86	8.97	9.04	6.08	5.29
Sn	<1	<1	4	3	3	1	2	2	1	6
Sr	403	290	200	226	462	88.2	128	99.2	1625	62.2
Ta	0.3	0.3	2.5	1.5	0.5	1.8	1.1	0.8	0.4	4.2
Tb	0.03	0.24	0.86	0.53	0.55	0.92	0.98	0.85	0.41	0.88
Th	1.06	3.71	19.5	18.55	18.8	60.1	60.5	62.4	9.17	33.3
Tm	0.01	0.17	0.39	0.2	0.16	0.22	0.37	0.2	0.13	0.4
U	0.24	1.97	2.36	2.56	22.6	11.65	7.07	10.1	0.98	6.02
V	<5	<5	60	18	15	12	11	6	17	8
W	1	1	2	1	1	1	1	1	1	2
Y	0.6	9.7	28.3	14.8	12.7	18.1	25.8	16.7	10	29.4
Yb	0.03	1.1	2.77	1.27	1.02	1.15	2.34	1.19	0.8	2.64
Zr	15	11	191	131	355	155	200	190	144	103

Table 3. Geochemical data from Tent Mountain and adjacent Humboldt Peak quadrangles (continued)

Sample	AZ7-29-20(2)	AZ7-28-20(4)	AZ 7-8-20 (1)	120720-9	060720-3	090720-1	110720-11	AZ8-19-19(6)	060720-4	AZ7-28-20(6)
Unit	Tmg	Tmg	Tmg	Tmg	Tmg	Tmg	Tmg	Tmg	Tqd	Tqd
Latitude	40.964633	40.990739	40.91403	40.6919	40.95022	40.91076	40.77194	40.95752	40.95022	40.98888
Longitude	-115.184384	-115.125656	-115.1092	-115.47	-115.221	-115.115	-115.294	-115.20163	-115.221	-115.141
Major and Minor Elements (%)										
SiO_2	72.80	75.10	73.80	74.50	75.30	70.70	74.20	72.20	69.20	62.70
Al2O3	14.25	14.20	13.85	13.80	14.15	15.90	14.00	14.30	16.05	17.60
FeO*	2.02	1.29	1.86	1.36	0.94	2.19	1.60	3.01	3.06	4.69
CaO	1.63	1.29	1.13	0.99	1.12	2.77	1.09	1.55	3.92	5.19
MgO	0.43	0.23	0.27	0.17	0.09	0.31	0.25	0.49	1.01	1.74
Na2O	3.39	3.78	2.87	3.01	3.62	3.90	3.39	2.84	3.75	3.57
K2O	4.27	4.01	5.24	5.04	5.06	2.71	4.80	5.21	1.31	1.59
Cr2O3	0.00	0.00	0.00	0.00	0.00	0.00	0.00	0.00	0.00	0.00
TiO2	0.24	0.10	0.17	0.13	0.04	0.18	0.14	0.41	0.41	0.56
MnO	0.05	0.04	0.03	0.01	0.06	0.03	0.03	0.03	0.05	0.07
P2O5	0.11	0.03	0.05	0.05	0.06	0.09	0.06	0.12	0.13	0.19
SrO	0.01	0.01	0.01	0.00	0.00	0.05	0.00	0.02	0.04	0.05
BaO	0.09	0.07	0.09	0.06	0.03	0.27	0.07	0.19	0.10	0.12
LOI	0.38	0.21	0.23	0.45	0.35	0.44	0.23	0.49	0.67	0.62
Total	99.29	100.16	99.37	99.12	100.47	99.10	99.63	100.37	99.03	98.07
Trace Elements (ppm)										
Ba	849	604	799	570	318	2520	652	1630	920	1075
Ce	70.3	83.6	132.5	98.1	33.8	110.5	83	275	83.1	54.6
Cr	10	20	10	20	10	10	10	10	20	20
Cs	2.69	8.29	0.87	0.91	1.17	4.9	2.23	0.82	2.28	1.37
Dy	3.49	7.78	4.17	13.65	4.37	1.58	3.75	5.58	1.45	3.11
Er	1.91	4.52	1.68	7.23	2.27	0.67	1.38	2.26	0.68	1.46
Eu	0.69	0.61	0.7	1.01	0.29	1.19	0.71	1.28	0.95	1.15
Ga	22.4	21.6	21.8	22.8	28.2	21.7	22.3	23.2	21.8	23.4
Gd	3.95	6.82	6.19	11.55	3.75	2.81	5.6	9.54	2.31	3.61
Hf	4.9	4.1	6.4	4.9	2.6	6.2	4.8	12.3	4.9	3.8
Ho	0.7	1.47	0.72	2.6	0.81	0.28	0.63	0.92	0.23	0.6
La	38.3	46.7	74.5	51.3	16.9	63.7	45	156.5	47.8	31.1
Lu	0.31	0.63	0.21	0.9	0.31	0.1	0.19	0.24	0.1	0.2
Nb	19	25	15.8	28.8	30.4	9.1	25.9	16	7.7	8.3
Nd	27	31.7	47	42.2	13.3	35.5	32.1	88.5	28.8	23.1
Pr	7.42	8.95	13.8	11.2	3.68	10.7	8.95	26.9	8.53	6
Rb	176.5	268	205	227	227	99.3	252	200	76.7	48.6
Sm	4.79	7.13	8.66	10.95	3.77	4.99	7.41	13.7	3.87	3.97
Sn	4	6	3	6	4	1	4	4	1	2
Sr	171.5	84.6	94.6	71.3	67.6	443	86	149.5	419	452
Ta	1.6	2.6	0.8	1.2	6.3	0.4	2.1	0.7	0.5	0.5
Tb	0.62	1.17	0.87	2.09	0.77	0.36	0.8	1.13	0.25	0.51
Th	21.6	42.9	62.3	50.6	18.45	18.95	45.1	91	12.75	7.09
Tm	0.27	0.67	0.25	0.99	0.36	0.11	0.21	0.29	0.09	0.2
U	5.28	7.25	8.56	8.1	5.04	1.96	8.59	3.46	1.53	1.31
V	27	9	12	11	<5	6	10	23	45	70
W	2	2	1	2	1	1	1	1	1	1
Y	19.6	44.3	18.2	74.4	23.1	7.1	16.4	24.3	6.9	15.7
Yb	2.1	4.34	1.38	5.89	2.21	0.7	1.36	1.64	0.6	1.35
Zr	161	125	197	140	59	239	149	473	177	155

Table 3. Geochemical data from Tent Mountain and adjacent Humboldt Peak quadrangles (continued)

Sample	AZ7-28-20(7)	AZ10-10-19(1)	AZ6-30-20(3)
Unit	Tqd	Tqd	Tqd
Latitude	40.988241	40.95913	40.94492
Longitude	-115.141195	-115.198767	-115.2036
Major and Minor Elements (%)			
SiO_2	70.70	64.90	69.10
Al2O3	15.40	16.30	15.65
FeO*	2.51	3.71	2.62
CaO	2.04	4.52	3.21
MgO	0.78	1.33	0.84
Na2O	3.42	4.31	3.14
K2O	3.65	2.21	3.62
Cr2O3	0.00	0.00	0.00
TiO2	0.38	0.44	0.29
MnO	0.04	0.09	0.05
P2O5	0.09	0.17	0.11
SrO	0.02	0.08	0.04
BaO	0.14	0.05	0.37
LOI	0.51	1.22	0.38
Total	99.17	98.11	99.04
Trace Elements (ppm)			
Ba	1315	465	3410
Ce	135.5	41.3	43.7
Cr	10	10	10
Cs	1.52	3.51	0.81
Dy	4.99	2.34	2.09
Er	2.43	1.18	1.21
Eu	1	0.92	0.77
Ga	25	18.9	19.9
Gd	6.9	2.77	2.4
Hf	8.1	3.5	4.2
Ho	0.86	0.43	0.4
La	75.3	20.5	25
Lu	0.39	0.2	0.18
Nb	18.5	5.1	5.7
Nd	50.3	18.5	17
Pr	14.3	4.89	4.72
Rb	129.5	53.5	63.6
Sm	9.44	3.58	3.02
Sn	1	1	1
Sr	222	667	417
Ta	1.2	0.2	0.5
Tb	1.03	0.41	0.36
Th	42.7	4.17	7.64
Tm	0.4	0.19	0.16
U	6.98	1.62	1.17
V	24	72	34
W	2	<1	1
Y	24.4	12.4	10.6
Yb	2.48	1.21	1.11
Zr	305	127	142

Samples analyzed at ALS Geochemistry in Reno, Nevada. Major element analyses were completed by fused bead and acid digestion preparation and analyzed using an inductively coupled plasma atomic emission spectroscopy (ICP-AES). Rare and trace element analyses were also completed by fused bead and acid digestion preparation and analyzed using an inductively coupled plasma mass spectrometer (ICP-MS).

Table 4. U-Pb zircon analyses from Arizona LaserChron

Spot	U (ppm)	206Pb 204Pb	U/Th	206Pb* 207Pb*	± (%)	Isotope ratios 207Pb* 235U*	± (%)	206Pb* 238U	± (%)	error corr.	Apparent ages (Ma) 206Pb* 238U*	± (Ma)	207Pb* 235U	± (Ma)	206Pb* 207Pb*	± (Ma)	Best age (Ma)	± (Ma)	Excl.[@]
Sample AZ8-19-19(6): Monzogranite (40.95752, -115.20163, 2170 m)																			
17r17	1335.8	41209.81	1.15	19.17	2.59	0.03432	2.99	0.00477	1.49	0.50	30.7	0.5	34.3	1.0	291.4	59.2	30.7	0.5	
8r8	1061.8	2784.52	23.05	23.91	1.29	0.02756	2.02	0.00478	1.55	0.77	30.8	0.5	27.6	0.5	NA	NA	30.8	0.5	
21r23	721.8	4853.72	1.42	22.27	1.79	0.02966	2.53	0.00479	1.79	0.71	30.8	0.5	29.7	0.7	NA	NA	30.8	0.5	
1r1	760.0	64959.16	0.74	19.43	1.52	0.03408	2.20	0.00481	1.59	0.72	30.9	0.5	34.0	0.7	260.5	34.9	30.9	0.5	
3r3	2275.2	73522.50	0.85	21.15	0.92	0.03143	1.46	0.00482	1.13	0.77	31.0	0.3	31.4	0.5	62.3	22.0	31.0	0.3	
22c24	769.1	308367.86	0.88	21.68	2.15	0.03069	2.51	0.00483	1.29	0.51	31.0	0.4	30.7	0.8	3.2	51.9	31.0	0.4	
9r9	1590.4	30513.87	1.06	20.88	1.53	0.03189	2.01	0.00483	1.31	0.65	31.1	0.4	31.9	0.6	92.9	36.2	31.1	0.4	
20r22	1882.1	14691.89	1.10	22.07	1.06	0.03017	1.65	0.00483	1.27	0.77	31.1	0.4	30.2	0.5	NA	NA	31.1	0.4	
13r13	1698.6	14478.65	0.83	20.62	1.32	0.03230	1.95	0.00483	1.44	0.74	31.1	0.4	32.3	0.6	122.4	31.1	31.1	0.4	
19c21	346.4	33190.88	1.47	22.49	2.76	0.02963	3.07	0.00484	1.35	0.44	31.1	0.4	29.7	0.9	NA	NA	31.1	0.4	
16r16	951.6	8744.12	1.35	20.45	2.01	0.03263	2.48	0.00484	1.45	0.59	31.1	0.5	32.6	0.8	142.0	47.2	31.1	0.5	
15r15	1200.8	29215.61	0.93	17.50	3.52	0.03827	3.88	0.00486	1.63	0.42	31.2	0.5	38.1	1.5	496.6	77.7	31.2	0.5	
10r10	2658.0	7737.01	1.04	22.20	0.99	0.03023	1.60	0.00487	1.25	0.78	31.3	0.4	30.2	0.5	NA	NA	31.3	0.4	
2r2	747.5	8006.45	1.07	21.25	2.32	0.03180	2.59	0.00490	1.16	0.45	31.5	0.4	31.8	0.8	51.6	55.4	31.5	0.4	
24c26	685.2	5725.10	1.68	21.21	3.24	0.03186	3.71	0.00490	1.80	0.49	31.5	0.6	31.8	1.2	55.6	77.2	31.5	0.6	
6r6	982.8	12879.42	1.15	16.93	5.42	0.03992	5.61	0.00490	1.44	0.26	31.5	0.5	39.7	2.2	568.8	118.1	31.5	0.5	
11r11	679.0	7978.89	1.26	22.09	1.84	0.03084	2.28	0.00494	1.36	0.59	31.8	0.4	30.8	0.7	NA	NA	31.8	0.4	
12r12	1119.4	15121.64	2.62	21.68	1.39	0.03149	2.16	0.00495	1.66	0.77	31.9	0.5	31.5	0.7	3.1	33.5	31.9	0.5	
18r18	1571.9	34309.97	0.91	21.24	1.55	0.03236	1.88	0.00499	1.07	0.57	32.1	0.3	32.3	0.6	52.7	37.0	32.1	0.3	
5r5	914.5	2255.37	0.91	18.19	7.15	0.03792	7.36	0.00500	1.74	0.24	32.2	0.6	37.8	2.7	410.3	160.1	32.2	0.6	
23r25	737.8	2494.45	1.31	23.21	2.02	0.02978	2.43	0.00502	1.35	0.55	32.3	0.4	29.8	0.7	NA	NA	32.3	0.4	
19r20	575.7	9108.51	1.60	21.46	2.06	0.03262	2.58	0.00508	1.56	0.60	32.7	0.5	32.6	0.8	27.8	49.4	32.7	0.5	x
4r4	928.0	10320.96	1.19	21.61	1.29	0.03246	2.01	0.00509	1.54	0.76	32.7	0.5	32.4	0.6	11.0	31.1	32.7	0.5	x
7r7	553.3	6233.36	1.41	20.88	2.07	0.03374	2.63	0.00511	1.61	0.61	32.9	0.5	33.7	0.9	92.8	49.1	32.9	0.5	x
14r14	483.3	2357.63	1.51	6.85	16.98	0.10924	17.19	0.00543	2.70	0.16	34.9	0.9	105.3	17.2	2299.0	294.1	34.9	0.9	x

[@]Analyses excluded from weighted mean calculation

Weighted mean age: 31.3 ± 0.2 Ma (n=21)
MSWD : 1.11

Laser ablation multicollector inductively coupled plasma mass spectrometry (LA-MC-ICPMS) analyses conducted at the Arizona LaserChron Center.
1. All uncertainties are reported at the 1-sigma level, and include only measurement errors.
2. Analyses conducted by LA-MC-ICPMS, as described by Gehrels et al. (2008).
3. U concentration and U/Th are calibrated relative to Sri Lanka zircon standard and are accurate to ~20%.
4. Common Pb correction is from measured 204Pb with common Pb composition interpreted from Stacey and Kramers (1975).
5. Common Pb composition assigned uncertainties of 1.5 for 206Pb/204Pb, 0.3 for 207Pb/204Pb, and 2.0 for 208Pb/204Pb.
6. U/Pb and 206Pb/207Pb fractionation is calibrated relative to fragments of a large Sri Lanka zircon of 563.5 ± 3.2 Ma (2-sigma).
7. U decay constants and composition as follows: 235U = 9.8485 x 10-10, 238U = 1.55125 x 10-10, 238U/235U = 137.88.
8. Weighted mean and concordia plots determined with Isoplot (Ludwig, 2008).

Table 5. U-Pb zircon analyses from UC Santa Barbara lab

			Isotope ratios					Apparent ages (Ma)					
Spot	U/Th	206Pb 204Pb	207Pb 235U	± (2s)	206Pb 238U	± (2s)	error corr.	206Pb* 238U*	± (Ma)	207Pb* 235U	± (Ma)	% Disc	Excl.*
Sample 060720-4 : Quartz diorite (40.950218, -115.220813, 1988 m)													
8	0.08	15454.5	0.038	0.0018	0.006	0.00025	0.99	37.8	1.4	38.1	1.5	0.8	x
2	0.87	2034.9	0.039	0.0016	0.006	0.00014	0.53	38.6	0.5	38.4	1.3	-0.6	
9	0.07	20151.4	0.040	0.0011	0.006	0.00014	0.88	38.7	0.5	39.7	0.7	2.4	
7	0.11	58000.0	0.040	0.0011	0.006	0.00014	0.72	39.1	0.5	39.9	0.8	2.0	
22	0.18	6733.3	0.040	0.0010	0.006	0.00014	0.74	39.1	0.4	39.5	0.6	0.9	
16	0.29	25033.3	0.039	0.0014	0.006	0.00014	0.10	39.1	0.4	39.3	1.2	0.5	
41	0.30	19203.1	0.039	0.0009	0.006	0.00013	0.82	39.1	0.3	39.0	0.5	-0.4	
21	0.27	2796.5	0.039	0.0015	0.006	0.00015	0.49	39.2	0.6	38.8	1.3	-1.0	
1	0.09	4664.7	0.040	0.0011	0.006	0.00015	0.95	39.2	0.6	39.5	0.7	0.8	
11	0.30	335.0	0.041	0.0018	0.006	0.00015	0.63	39.3	0.6	40.4	1.6	2.8	
42	0.23	2500.0	0.040	0.0014	0.006	0.00016	0.52	39.3	0.7	39.6	1.2	0.9	
6	0.09	3863.0	0.043	0.0011	0.006	0.00013	0.77	39.4	0.4	42.5	0.7	7.1	
8	0.22	2920.0	0.040	0.0014	0.006	0.00016	0.03	39.3	0.7	39.8	1.1	1.2	
32	0.23	3611.9	0.040	0.0011	0.006	0.00014	0.52	39.4	0.5	40.1	0.7	1.8	
19	0.22	184.1	0.041	0.0016	0.006	0.00016	0.36	39.5	0.6	40.4	1.4	2.3	
23	0.29	3327.3	0.042	0.0011	0.006	0.00014	0.72	39.5	0.4	42.2	0.7	6.3	
40	0.30	4905.1	0.040	0.0010	0.006	0.00013	0.25	39.4	0.3	39.7	0.6	0.7	
29	0.18	-909.3	0.041	0.0014	0.006	0.00016	0.42	39.5	0.7	40.4	1.1	2.3	
25	0.39	2654.1	0.041	0.0014	0.006	0.00013	0.10	39.5	0.3	41.2	1.1	4.1	
63	0.27	4455.1	0.041	0.0012	0.006	0.00015	0.61	39.5	0.5	40.3	0.9	2.0	
26	0.36	-19166.7	0.039	0.0014	0.006	0.00014	0.51	39.5	0.5	39.3	1.0	-0.5	
43	0.49	4641.8	0.041	0.0013	0.006	0.00015	0.31	39.6	0.5	40.3	0.9	2.0	
24	0.18	40682.9	0.040	0.0010	0.006	0.00014	0.66	39.6	0.5	39.8	0.7	0.4	
5	0.22	2533.8	0.040	0.0033	0.006	0.00017	0.73	39.7	0.8	40.1	3.1	1.1	
56	0.25	2013.8	0.042	0.0014	0.006	0.00013	0.44	39.8	0.3	41.7	1.1	4.6	
18	0.26	2896.3	0.039	0.0013	0.006	0.00014	0.36	39.6	0.4	39.2	1.0	-1.0	
46	0.40	2178.6	0.042	0.0015	0.006	0.00013	0.23	39.8	0.3	42.1	1.1	5.5	
49	0.21	985.5	0.040	0.0015	0.006	0.00014	0.31	39.7	0.5	40.0	1.2	0.7	
33	0.30	-28458.3	0.040	0.0012	0.006	0.00015	0.51	39.7	0.6	40.1	0.9	1.1	
47	0.28	1165.4	0.040	0.0015	0.006	0.00017	0.62	39.7	0.8	39.7	1.3	0.0	
41	0.35	553.1	0.040	0.0031	0.006	0.00017	0.47	39.8	0.7	40.2	2.9	1.0	
28	0.36	1052.3	0.041	0.0022	0.006	0.00023	0.58	39.8	1.2	40.7	2.0	2.2	
36	0.18	8355.6	0.040	0.0010	0.006	0.00015	0.85	39.8	0.6	40.3	0.7	1.2	
58	0.40	94866.7	0.040	0.0009	0.006	0.00014	0.57	39.8	0.5	40.0	0.5	0.4	
51	0.33	1190.8	0.040	0.0013	0.006	0.00017	0.64	39.8	0.7	39.6	1.0	-0.5	
55	0.27	15051.7	0.040	0.0011	0.006	0.00014	0.78	39.8	0.5	40.0	0.7	0.3	
42	0.44	27280.0	0.041	0.0009	0.006	0.00014	0.83	39.9	0.4	40.4	0.4	1.2	
44	0.24	4240.6	0.041	0.0015	0.006	0.00015	0.50	39.9	0.5	40.6	1.1	1.7	
45	0.57	3262.5	0.041	0.0014	0.006	0.00018	0.82	40.0	0.9	40.8	1.1	2.0	
31	0.20	12844.7	0.041	0.0010	0.006	0.00013	0.78	40.0	0.3	40.9	0.5	2.2	
12	0.07	22544.4	0.041	0.0010	0.006	0.00014	0.87	40.0	0.4	40.5	0.5	1.1	
3	0.53	1958.2	0.040	0.0016	0.006	0.00015	0.46	40.0	0.5	39.4	1.4	-1.4	
65	0.22	5400.0	0.040	0.0014	0.006	0.00014	0.56	40.0	0.4	39.5	1.1	-1.2	
9	0.23	4506.2	0.040	0.0012	0.006	0.00014	0.70	40.0	0.4	40.0	0.9	-0.2	
39	0.30	2113.9	0.041	0.0012	0.006	0.00014	0.10	40.0	0.4	40.6	0.9	1.3	
24	0.20	14615.4	0.041	0.0015	0.006	0.00016	0.92	40.1	0.7	40.7	1.1	1.4	
66	0.50	2105.3	0.042	0.0015	0.006	0.00015	0.29	40.2	0.5	41.6	1.3	3.3	
62	0.35	-15973.7	0.040	0.0015	0.006	0.00015	0.47	40.1	0.5	39.7	1.2	-1.1	
7	0.25	2005.7	0.041	0.0016	0.006	0.00015	0.66	40.2	0.5	41.0	1.4	1.9	
4	0.22	1514.7	0.041	0.0011	0.006	0.00015	0.86	40.2	0.6	41.0	0.7	1.9	
10	0.22	2823.5	0.040	0.0011	0.006	0.00013	0.30	40.2	0.3	39.6	0.7	-1.5	
54	0.25	24660.7	0.041	0.0011	0.006	0.00014	0.71	40.4	0.4	41.0	0.7	1.6	
28	0.46	3806.3	0.041	0.0015	0.006	0.00019	0.76	40.4	0.9	41.2	1.3	1.9	
53	0.10	2310.2	0.045	0.0020	0.006	0.00014	0.01	40.8	0.4	44.4	1.8	8.2	
13	0.35	1341.5	0.043	0.0017	0.006	0.00015	0.18	40.6	0.5	42.6	1.4	4.6	
68	0.12	21870.5	0.041	0.0010	0.006	0.00015	0.90	40.7	0.5	40.8	0.6	0.4	
33	0.06	3302.0	0.041	0.0011	0.006	0.00014	0.82	40.7	0.4	41.2	0.7	1.2	
5	0.25	9620.8	0.041	0.0012	0.006	0.00017	0.67	40.8	0.7	40.6	0.9	-0.5	
60	0.23	18042.9	0.041	0.0009	0.006	0.00014	0.65	40.8	0.4	40.7	0.5	-0.2	
1	0.45	1702.9	0.041	0.0012	0.006	0.00015	0.25	40.8	0.5	40.9	0.9	0.1	
30	0.44	2132.6	0.042	0.0011	0.006	0.00016	0.08	41.1	0.6	42.0	0.6	2.4	
48	0.32	19230.8	0.042	0.0014	0.006	0.00016	0.10	41.1	0.7	41.4	1.1	0.8	
27	0.13	9125.0	0.042	0.0012	0.006	0.00017	0.85	41.0	0.7	41.6	0.8	1.3	
67	0.27	15074.5	0.041	0.0011	0.006	0.00016	0.87	41.1	0.6	40.4	0.7	-1.7	
27	0.18	4013.5	0.042	0.0017	0.006	0.00021	0.66	41.2	1.1	41.4	1.5	0.5	
20	0.12	3594.8	0.044	0.0017	0.006	0.00015	0.25	41.4	0.5	43.6	1.3	5.0	
38	0.41	5344.8	0.043	0.0010	0.007	0.00017	0.37	41.8	0.7	42.6	0.5	1.9	
50	0.41	3923.8	0.041	0.0012	0.007	0.00017	0.73	41.9	0.7	41.3	0.9	-1.6	
37	0.24	4122.6	0.044	0.0012	0.007	0.00016	0.10	43.2	0.6	43.6	0.9	1.1	x
11	0.14	7322.6	0.045	0.0013	0.007	0.00016	0.35	43.9	0.5	44.8	0.9	1.8	x
30	0.08	-7040.0	0.046	0.0020	0.007	0.00030	0.89	45.3	1.7	45.4	1.8	0.2	x

@Analyses excluded from weighted mean calculation

Weighted mean age: 39.9 ± 0.2 Ma (n=67)

MSWD : 1.9

Analyses conducted at the UC Santa Barbara using the Nu Instruments Plasma HR-ES multicollector ICP with a 193 nm ArF excimer laser ablation system. Analytical procedures followed that of McKinney et al. (2015). Spot diameters were 20 um. The primary standard used was 91500. Secondary standards include 9435, AusZ, Plesovice, GJ-1, R33 and Tem2. Iolite3 was used to reduce data following the scheme of Paton et al. (2010). For this preliminary analysis, xenocrystic zircons with ages >50 Ma or discordant grains (>10% normal discordance) were excluded from the datatable. Analysis by Drew A. Levy.